Biochimica et Biophysica Acta 1840 (2014) 350–356

Contents lists available at ScienceDirect

Biochimica et Biophysica Acta

journal homepage: www.elsevier.com/locate/bbagen

Nucleic acid binding properties of allicin: Spectroscopic analysis and estimation of anti-tumor potential

Gunjan Tyagi [a], Shrikant Pradhan [b], Tapasya Srivastava [b,*], Ranjana Mehrotra [a,**]

[a] Quantum Optics and Photon Physics, CSIR—National Physical Laboratory, Dr. K.S. Krishnan Marg, New Delhi 110 012, India
[b] Department of Genetics, University of Delhi (South Campus), New Delhi 110 021, India

ARTICLE INFO

Article history:
Received 21 April 2013
Received in revised form 3 August 2013
Accepted 6 September 2013
Available online 13 September 2013

Keywords:
Deoxyribonucleicacid
Ribonucleicacid
Allicin
Fourier transform infrared spectroscopy
MTT

ABSTRACT

Background: Allicin has received much attention due to its anti-proliferative activity and not-well elucidated underlying mechanism of action. This work focuses towards determining the cellular toxicity of allicin and understanding its interaction with nucleic acid at molecular level.
Methods: MTT assay was used to assess the cell viability of A549 lung cancer cells against allicin. Fourier transform infrared (FTIR) and UV-visible spectroscopy were used to study the binding parameters of nucleic acid-allicin interaction.
Results: Allicin inhibits the proliferation of cancer cells in a concentration dependent manner. FTIR spectroscopy exhibited that allicin binds preferentially to minor groove of DNA via thymine base. Analysis of tRNA allicin complex has also revealed that allicin binds primarily through nitrogenous bases. Some amount of external binding with phosphate backbone was also observed for both DNA and RNA. UV visible spectra of both DNA allicin and RNA allicin complexes showed hypochromic shift with an estimated binding constant of 1.2×10^4 M^{-1} for DNA and 1.06×10^3 $M^{-1}$for RNA binding. No major transition from the B-form of DNA and A-form of RNA is observed after their interaction with allicin.
Conclusions: The results demonstrated that allicin treatment inhibited the proliferation of A549 cells in a dose-dependent manner. Biophysical outcomes are suggestive of base binding and helix contraction of nucleic acid structure upon binding with allicin.
General significance: The results describe cytotoxic potential of allicin and its binding properties with cellular nucleic acid, which could be helpful in deciphering the complete mechanism of cell death exerted by allicin.

1. Introduction

Allicin, diallylthiosulfinate, is an organosulfur compound known for its effective medicinal properties [1] (Fig. 1). It is regarded as a principle biological active component of garlic. Allicin was isolated in the middle of 20th century and was first recognized for its antibacterial properties [2]. Discovery of allicin is regarded as a leap forward in deciphering the health benefits associated with garlic. So far much research has been conducted on this medicinal compound and it is known for its antibacterial, anti-inflammatory and anti-oxidant properties along with cardiovascular benefits [3–5]. Since last few decades several studies have also linked allicin to tumor inhibition. Scientific investigations have demonstrated that allicin is capable of arresting rapidly dividing cells and can elicit their death. It has been reported to induce cell death by triggering apoptosis through mitochondrial pathway in HL60 and U937 cells [6]. Allicin was found to induce apoptosis in human cervical cancer SiHa cells and mouse fibroblast-like L-929 cells, through the appearance of characteristic apoptotic bodies, DNA fragmentation, and activation of caspases [7]. Growth of human epithelial carcinoma cell lines was also inhibited by allicin through a caspase-independent pathway, mediated by protein kinase A (PKA) activation and release of flavoprotein, AIF (apoptotic-inducing factor) from mitochondria [8]. Many other studies also attribute the cell death in various cancer cell lines and inhibition of induced tumor in animals to the anticancer action of allicin. However, the underlying mechanism of cell death caused by allicin has not been precisely and completely interpreted.

Several lines of evidence have indicated that allicin and its related compounds exert significant effect on cellular nucleic acid as a part of their anti-cancer mechanism. It is known to induce DNA fragmentation in various cell lines. S. Oommen et al. have shown the decrease in the rate of DNA synthesis as a function of increased concentration of allicin [7]. Several DADS (di allyl disulfide) analogues have been recognized to bind DNA [9]. It has also been realized that allicin reacts with RNA polymerase [10] and induces suppression of certain mRNA levels in human monocytes [11]. On the basis of these observations we have assessed the activity of allicin against A549 human non-small cell lung adenocarcinoma cell line and investigated the possibility of allicin interaction

* Corresponding author. Tel.: +91 11 24112761.
** Corresponding author. Tel.: +91 11 45608366; fax: +91 11 45609310.
E-mail addresses: tapasya@south.du.ac.in (T. Srivastava), ranjana@nplindia.org (R. Mehrotra).

0304-4165/$ – see front matter © 2013 Elsevier B.V. All rights reserved.
http://dx.doi.org/10.1016/j.bbagen.2013.09.007

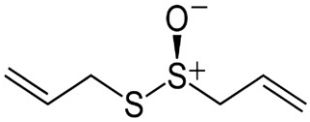

Fig. 1. Chemical structure of allicin.

with DNA and RNA by using FTIR difference spectroscopy and UV-vis absorption spectroscopy. FTIR spectroscopy has solved various problems related to biological macromolecular complexes [12–14]. It has emerged as an efficient tool in characterizing the nature of various biomolecules and their complexes, particularly for their structural information [15]. Precisely, it has shown tremendous potential in deciphering the binding parameters of various DNA-ligand and RNA-ligand complexes [16–19]. Hence in this study we have used the potential of FTIR and UV-vis spectroscopy to analyze various binding parameters of allicin DNA and allicin RNA complexes.

2. Materials and methods

2.1. Materials

Calf thymus DNA (Type I, sodium content 6%) and tRNA from Baker's yeast were purchased from Sigma-Aldrich chemicals (USA). Allicin was procured from Allicin International Ltd. Purity of DNA and RNA were estimated by recording the UV absorbance at 260 and 280 nm and calculating ratio, A_{260}/A_{280}. The ratio was found to be more than 1.9, indicating that the DNA and RNA are free from protein [20]. Deionized water from the Millipore water purification system was used in the preparation of desired aqueous solutions. Other chemicals and reagents used in the study were of analytical grade and used as supplied.

2.2. Preparation of stock solutions

Solution of DNA and RNA sodium salt was prepared in 10 mM Tris-HCl buffer (pH 7.4) and kept at 8 °C for 24 h. The solution was stirred at frequent intervals to ensure its homogeneity. Concentration of DNA and RNA stock solutions was measured spectrophotometrically using excitation coefficient of 6600 cm^{-1} M^{-1} and 9250 cm^{-1} M^{-1} respectively [21]. The final concentration of DNA and RNA stock solutions was 25 mM. For FTIR studies allicin–DNA and allicin–RNA complex solutions were prepared, so as to attain the allicin/DNA and allicin/RNA molar ratios (r) of 1/150, 1/80 and 1/20 with varying concentration of allicin and constant concentration of DNA and RNA. UV visible studies were carried out using allicin concentrations ranging from 0.025 mM to 0.5 mM and DNA and RNA concentration of 2.5 mM.

2.3. Cell culture and cell viability

The human non-small cell lung adenocarcinoma cell line A549 was used in the study. Cells were cultured in Dulbecco's modified Eagle's medium (DMEM) (Sigma, USA) supplemented with 10% fetal bovine serum (Himedia, India) and 10 μg/ml ciprofloxacin (Sigma, USA). Cells were incubated at 37 °C in 5% CO_2 atmosphere.

Cell viability was measured using the MTT assay. A549 cells were plated at a density of 5×10^3 cells per well in 96 well plates. After overnight culture, cells were treated with different concentrations of allicin (1, 10, 20, 40, 60, 80, 100, 120, 150 μg/ml) and incubated in cell culture conditions for 72 h at 37 °C. Then, medium in each well was discarded and 100 μl media containing 200 μg/ml MTT was added in each well and the plates were incubated at 37 °C for 4 h. The medium containing MTT was discarded and 200 μl DMSO was added to dissolve the insoluble purple formazan product to colored solution. Absorbance was recorded at 570 nm. Allicin mediated cell death was assessed by comparing the viability of treated cells with that of untreated control cells using the following formula.

$$\text{Cell Viability } \% = \frac{[\text{Absorbance of a well with cells}] - [\text{Mean absorbance of media blank well}]}{\text{Mean absorbance in } [\text{control wells} - \text{media blank well}]} \times 100$$

The experiments were performed in three biological replicates.

2.4. FTIR spectral measurements

FTIR spectra were recorded with Varian 660-IR spectrophotometer, equipped with DTGS (deuterated triglycine sulphate) detector and KBr beam splitter. All spectra were recorded in 10 milli molar Tris-HCl buffer as a solvent (pH of 7.4). Liquid samples were analyzed in attenuated total reflectance mode with ZnSe crystal. Ambient humidity of 45% RH was maintained during the experiment. A total of 256 scans were recorded for each sample in the spectral range of 4000-650 cm^{-1} with a resolution of 4 cm^{-1}. Background spectra were collected before each measurement. A spectrum of buffer solution was recorded and subtracted from the spectra of DNA, RNA and allicin DNA and allicin RNA complexes. A satisfactory buffer subtraction was considered to be achieved when the intensity of water combination band at about 2200 cm^{-1} became zero in all the spectra recorded [22]. FTIR difference spectra were produced by subtracting the spectrum of free DNA from the spectrum of allicin DNA complex ((DNA solution + allicin solution) − (DNA solution)).

2.5. UV–visible spectral measurements

The UV–visible spectra were recorded on Perkin Elmer spectrophotometer, Lambda 35. Quartz cuvettes of 1 cm path length were used for measurement. Spectra were recorded for free DNA, RNA and for various allicin–DNA and allicin–RNA complex solutions. For the calculation of the binding constant of the reaction occurring between allicin and DNA and allicin and RNA the method described by Kanakis et al. [23] is used. It is presumed that after the interaction between ligand [L], which is allicin and substrate [S] which is DNA and/or RNA in aqueous solution, the complex [SL] forms [24].

It is also assumed that the substrate and the ligand follow beer's law for the absorbance of light. The absorbance of substrate solution at its total concentration with a path length [l] of 1 cm is

$$A_o = \varepsilon_s l S_t \tag{1}$$

ε_s is the molar absorptivity of DNA.

The absorbance of solution consisting of total concentration of substrate along with total concentration of ligand is

$$A_L = \varepsilon_S l[S] + \varepsilon_L l[L] + \varepsilon_{SL} l[\mathrm{SL}]. \tag{2}$$

[S] is the concentration of uncomplexed substrate.
[L] is the concentration of uncomplexed ligand.
[SL] is the concentration of substrate-ligand complex.
ε_L is the molar absorptivity of ligand.

After combining with the mass balance of substrate and ligand, the absorbance equation can be written as

$$A_L = \varepsilon_S l S_t + \varepsilon_L l L_t + \Delta\varepsilon_{SL} l[\mathrm{SL}] \tag{3}$$

$$\Delta\varepsilon_{SL} = \varepsilon_{SL} - \varepsilon_S - \varepsilon_L.$$

The absorbance of solution measured against the total concentratin of ligand as reference is

$$A = \varepsilon_S l S_t + \Delta\varepsilon_S l[\mathrm{SL}] \tag{4}$$

The stability constant for the formation of complex [SL] can be given as

$$K_{SL} = [SL]/[S][L] \tag{5}$$

Combining Eqs. (4) and (5)

$$\Delta A = K_{SL}\Delta\varepsilon_{SL} l[S][L] \tag{6}$$

$$\Delta A = A_0 - A$$

From the mass balance equation $S_t = [S] + [SL]$ we get $[S] = S_t/[1 + K_{SL}[L]]$, which gives Eq. (7)

$$\frac{\Delta A}{l} = \frac{S_t K_{SL}\varepsilon_{SL}[L]}{1 + K_{SL}[L]} \tag{7}$$

This shows the hyperbolic dependence of binding on free ligand concentration. Linear transformation of Eq. (6) is done by taking the reciprocal of each side of Eq. (7).

$$\frac{l}{\Delta A} = \frac{1}{S_t K_{SL}\Delta\varepsilon_{SL}[L]} + \frac{1}{S_t\Delta\varepsilon_{SL}} \tag{8}$$

The double reciprocal plot of $1/\Delta A$ versus $1/[L]$ is linear and the binding constant $[K]$ can be estimated by calculating the ratio of the intercept to the slope.

3. Results and Discussion

3.1. Effect of allicin on growth of A549 cells

Cytotoxic potential of allicin is tested against A549 lung cancer cell lines using MTT assay. Cell viability assessed after 72 h of treatment shows that allicin inhibits the growth of A549 cells in a concentration dependent manner. For each dose six replicates were taken and the experiment was repeated three times with similar results. Fig. 2 represents the allicin dose-response survival curve of A549 cells. The low dose of allicin, 1.0 μg/ml showed approximately 15% cytotoxicity after 72 h of treatment. The concentration of allicin, which resulted in 50% cell population mortality, is ~30 μg/ml. While the highest concentration of allicin leads to ~85% cell death in three biological replicates.

3.2. Allicin–DNA complex

3.2.1. FTIR measurements and analysis

Infrared marker bands in the region 1800 cm^{-1}–700 cm^{-1} provide information about the various portion of double helical DNA structure. Careful observation of the changes occurring in these marker bands gives important information about the base pairing, stacking, helix conformation and sugar orientation in the DNA structure. In the present experiment guanine band occurs at 1715 cm^{-1}, which is attributed to its C6—O6 ring vibrations (Fig. 3). The position at 1656 cm^{-1} is attributed to C O vibrations of thymine, present in the minor groove of DNA, while the frequency position at 1609 cm^{-1} is assigned to adenine bases. Cytosine infrared vibrations occur at 1493 cm^{-1}. Asymmetric and symmetric phosphate vibrations occur at 1221 and 1084 cm^{-1}. At the band position of 837 cm^{-1}, the marker band of B-DNA due to deoxyribose stretching has been marked. These are the remarkable infrared bands, representative of DNA double helix, which are observed during allicin–DNA interaction at different ratios.

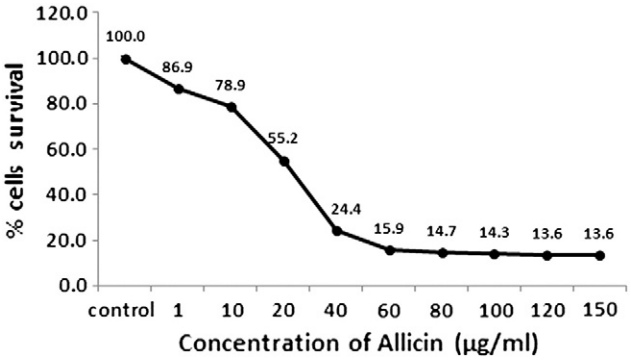

Fig. 2. Dose response cell survival curve of A549 cells against allicin. Each point represents the data of three biological replicates, containing hexaplate samples. The error bars indicate standard deviations.

Evidence of allicin–DNA complex formation derives from the shifting of the infrared band at 1656 cm^{-1} to higher wavenumber 1660 cm^{-1} along with its splitting into two bands (Fig. 3). Shifting and splitting of the peak assigned to thymine indicates towards allicin binding to the thymine oxygen present in the minor groove of DNA helix. Along with the changes observed at 1656 cm^{-1}, a new band centered around 1689 cm^{-1} is observed in allicin–DNA complexes (Fig. 4a). Observation of infrared spectrum of free allicin (Supplementary Fig. 1) confirms that this new band does not belong to allicin and is thus attributed to allicin–DNA complex. This band is assigned to thymidine carbonyl group located in the minor groove of DNA and illustrates intensity increment upon interaction with ligand [25,26]. The position of this band is further clear in second derivative spectra of DNA and allicin–DNA complexes (Fig. 4b). Second derivatives are specifically useful for accurate determination of band positions of biomolecules in free and complex forms as well as for resolving overlapping bands. We have also generated second derivate spectra in the region 1800 cm^{-1}–700 cm^{-1} for position confirmation of infrared bands of allicin–DNA complex (Supplementary Fig. 2), which intrinsically illustrates the shifting and intensity variation of major infrared bands of DNA.

Furthermore, significant shift is observed for guanine band from 1715 to 1711 cm^{-1}. Shift and intensity variation in guanine band may be due to indirect effect of allicin interaction with thymine group in minor groove. It should be noted that any ligand interaction in DNA groove (minor or major) might result in change in the ratio of minor/major groove width and hence, change in frequency of groove sensitive infrared bands. Asymmetric phosphate band exhibit a shift of 3 cm^{-1} from 1221 cm^{-1} to 1224 cm^{-1} at $r = 1/20$ molar ratio, while the symmetric phosphate vibration at 1084 cm^{-1} shifts to 1086 cm^{-1} along with an appreciable intensity variation. Intensity changes of the infrared bands are estimated from the positive and negative features appearing in the difference spectra of allicin–DNA complexes (Fig. 5). Along with changes in wavenumber position, variation in band intensity as an effect of allicin binding on three cardinal IR bands, representative of reactive sites located in the minor groove (thymine 1656 cm^{-1}), major groove (guanine 1715 cm^{-1}) and on the backbone of DNA (asymmetric PO2, 1221 cm^{-1}) has also been calculated in terms of percentage (Fig. 6). Taking all these points together, major effect of allicin is found on thymine after its complex formation with DNA. These results indicate towards the minor groove binding of allicin with some amount of external interaction with negatively charged phosphate backbone. The observations are supported by the fact that small flat and crescent shape molecules prefer minor groove binding [27] and allicin is a flat molecule with a curvature in its structure. Infrared bands that are assigned to adenine and cytosine at 1609 and 1493 cm^{-1} exhibit negligible changes and suggest no major interaction of allicin at these sites.

3.2.2. UV–visible absorption measurements and analysis

In the UV–visible characterization of DNA–drug binding the band at 260 nm arises due to π–π* transition of DNA nitrogenous bases. Variation in absorbance and wavelength shift of this band reflect the structural changes occurring in DNA upon drug complexation. In the present situation there occurs an initial gradual decrease in DNA absorption band (hypochromic effect) at 260 nm when low concentration of allicin

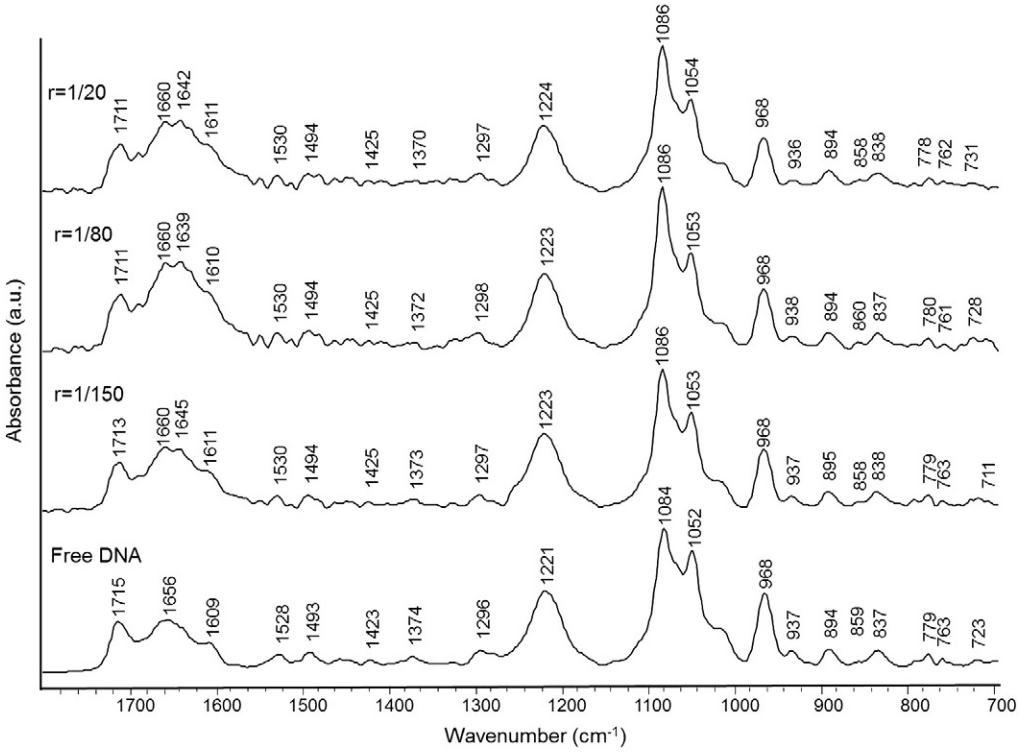

Fig. 3. FTIR spectra in the region of 1800–700 cm^{-1} for free DNA and allicin–DNA complexes.

is complexed with DNA (Fig. 7). While at high concentration of allicin an increase in the absorption of 260 nm peak is observed with slight change in absorption maxima. The spectral deviations observed reflect the changes occurring in the structure of DNA with increasing concentration of allicin. Initial hypochromic effect suggests contraction of DNA helix due to binding of allicin with DNA bases and phosphate backbone. The reactive cationic group of allicin [28] might have electrostatically interacted with negatively charged phosphate group of DNA backbone resulting in the helix contraction which is evident from decrease in its UV absorption band. Hyperchromism at increased allicin concentration may have occurred due to dimerization or some other effect causing some degree of helix intercalation. Similar results are also observed in case of diorganotin [29] and polymeric Schiff's base binding with DNA [30]. The stability of the allicin–DNA complex is assessed by calculating the binding constant of the reaction between allicin and DNA using the method described in experimental section. The observed binding constant in the concentration range of 0.025 mM to 0.5 mM of allicin is $K = 1.2 \times 10^4\ M^{-1}$ (Fig. 7). The order of the binding constant is suggestive of moderate binding of allicin with DNA.

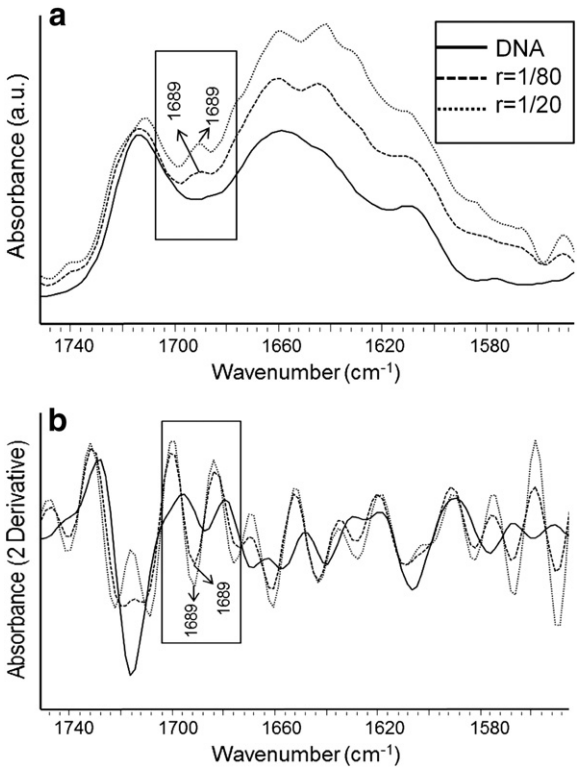

Fig. 4. (a) Overlaid FTIR spectra in the region 1800–1500 cm^{-1}. (b) Overlaid FTIR second derivative spectra, in the region 1800–1500 cm^{-1}.

3.3. Allicin–RNA complex

3.3.1. FTIR measurements and analysis

The infrared spectrum of tRNA appears similar to double stranded DNA in A-form. Fig. 8 represents the frequencies of important units of tRNA. Infrared vibrations appearing between 1700 and1500cm^{-1} were assigned to the in-plane vibration of RNA bases. The strong infrared band at 1700 cm^{-1} is assigned to the C O and C N stretching vibrations of guanine residues. The other strong band at 1650 cm^{-1} is primarily assigned to the C O stretching vibrations of uracil. Band appearing at the position 1602 cm^{-1} is allocated to the adenine residues. Other infrared bands associated to RNA vibrations in the region between 1500 and 1250 cm^{-1} are assigned to the in-plane ring vibrations of the bases and contain some marker of A-form RNA. A prominent absorption band is located at 1489 cm^{-1}, which is attributed to cytosine in-plane ring vibrations.

Conspicuous bands in the region 1250–1080 cm^{-1} of the tRNA spectrum correspond to backbone phosphate group vibrational frequencies. Strong absorption bands located at 1237 and 1086 cm^{-1} are assigned mainly to the asymmetric and symmetric stretching vibrations of the PO2 groups, respectively. The spectral region of

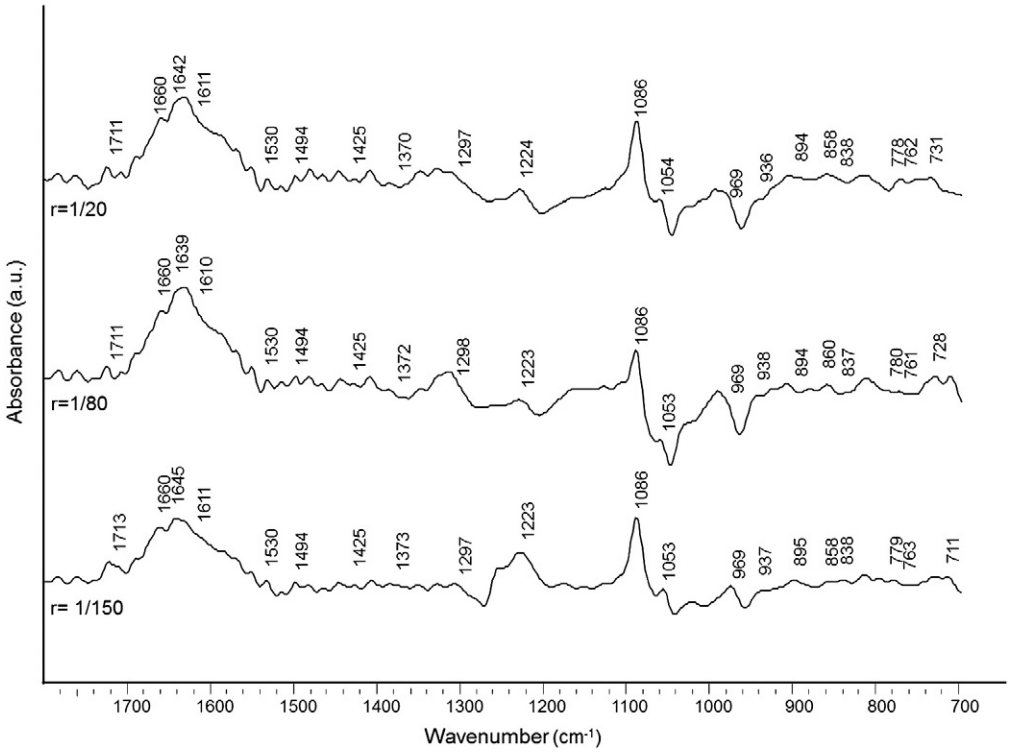

Fig. 5. Difference spectra {(DNA solution + allicin solution) − DNA solution)} of allicin–DNA complexes in the region of 1800–700 cm^{-1}.

1080–800 cm^{-1}comprises of various infrared marker bands of tRNA in A-conformation, attributed to phosphodiester chain conjoined with ribose sugar vibrational modes. The infrared spectral features of tRNA–allicin complexes are shown in Fig. 8. Major shifting of the infrared absorption bands of pure tRNA is observed in the base region upon allicin complexation. The band at 1700 cm^{-1}which is ascribed to guanine vibrations underwent shifting to higher wavenumber along with increase in its intensity after its binding with tRNA. The other significant shift is observed for the band of uracil (C O) located at 1650 cm^{-1}. A noteworthy increase in the relative intensity of IR absorption band is also observed for this band (Fig. 9). Adenine band at 1602 cm^{-1} exhibited a higher wavenumber shift when high concentration of allicin is complexed with tRNA. Cytosine band at 1489 cm^{-1} did not demonstrate any profound change in its frequency position after the formation of tRNA–allicin complex, although some intensity variation is observed for this band. In the phosphate region only at high allicin concentration an appreciable shift of 3 cm^{-1} is observed from 1237 to 1240 cm^{-1} while the other band at1086cm^{-1} did not show any wavenumber shift. However some intensity change is observed for these bands in the difference spectra. Second derivative spectra have also been generated for allicin–RNA complex for position determination of infrared bands (Supplementary Fig. 3).

3.3.2. UV–visible absorption measurements and analysis

UV–visible absorption of tRNA in the presence of varying concentration of allicin is shown in Fig. 10. Spectral variations were measured by following changes in the absorption at 260 nm which is characteristic of tRNA. When the molar ratio of tRNA/allicin is low the electronic

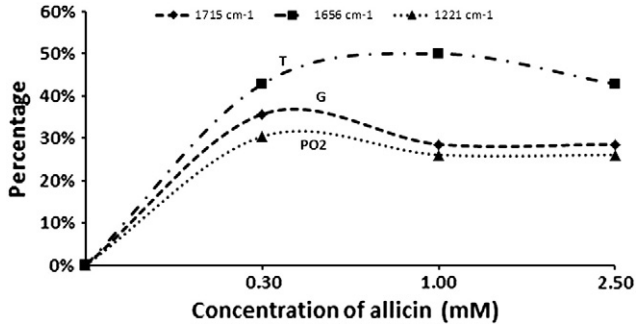

Fig. 6. Percentage effect of allicin on minor groove (mainly thymine (T), 1656 cm^{-1}), major groove (mainly guanine (G), 1715 cm^{-1}) and sugar phosphate backbone (PO2) (1221 cm^{-1}) of DNA as a function of allicin concentration.

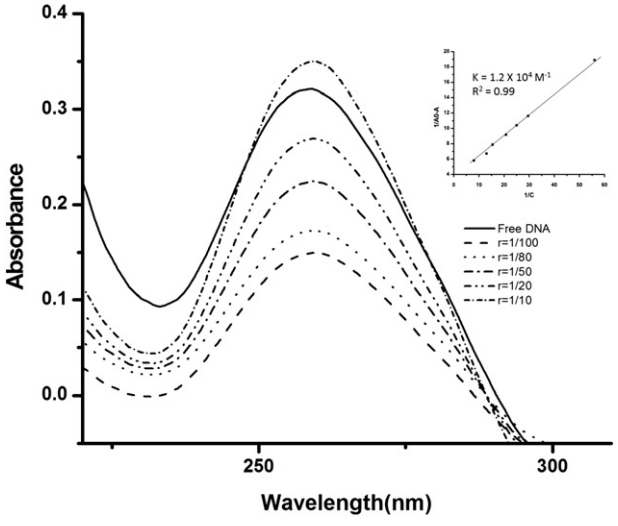

Fig. 7. UV–visible spectra of free DNA and DNA–allicin complexes at 260 nm. Plot of $1/(A_0 - A)$ versus $1/C$ for DNA and its drug complexes, where A_0 is the initial absorption of DNA and A is the recorded absorption at different drug concentrations.

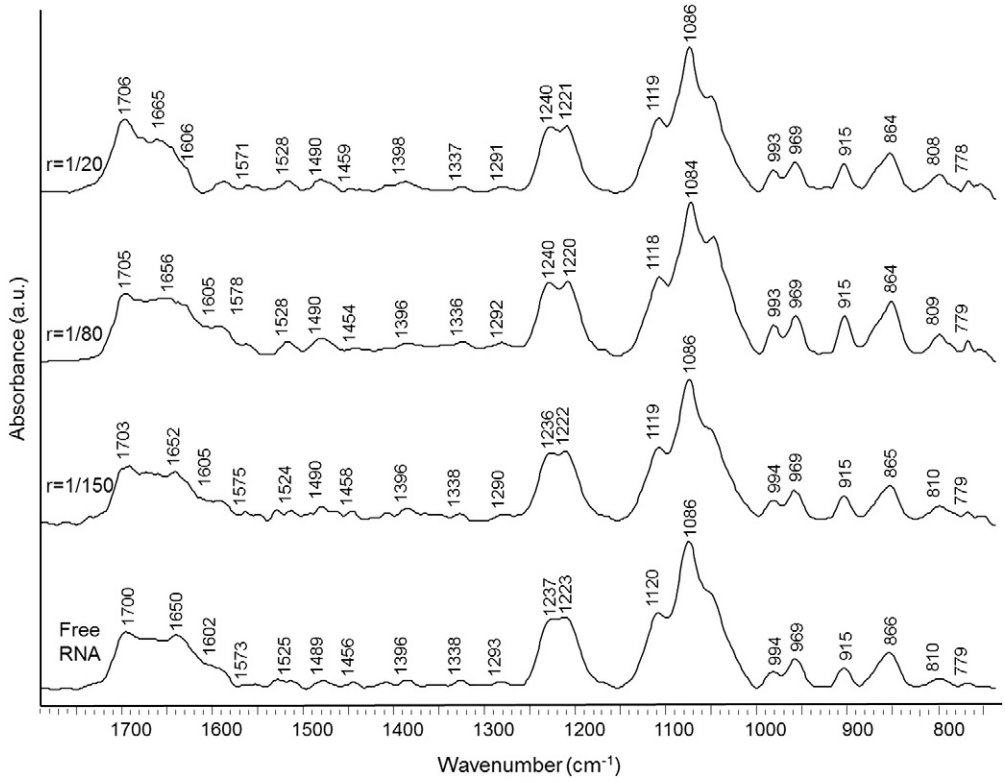

Fig. 8. FTIR spectra in the region of 1800–700 cm^{-1} for free tRNA and allicin–tRNA complexes.

absorption intensity of tRNA began to decrease leading to the hypochromic effect. But when the ratio is relatively high the absorption began to increase. The UV–visible spectral changes are consistent with the FTIR results. According to our observation at low concentration the reactive electrophilic groups of allicin react with tRNA base and negatively charged phosphate backbone. Further interaction at high allicin concentration might have led to some intercalation in to the tRNA duplex, which is credited to the hyperchromic effect. The intrinsic binding constant calculated for the estimation of tRNA–allicin complex stability is found to be $K = 1.06 \times 10^3 M^{-1}$.

The order of the binding constant is indicative of weak to moderate binding of allicin with tRNA. Together the results of FTIR and absorption spectroscopy suggest allicin binding primarily to the nitrogenous bases of tRNA.

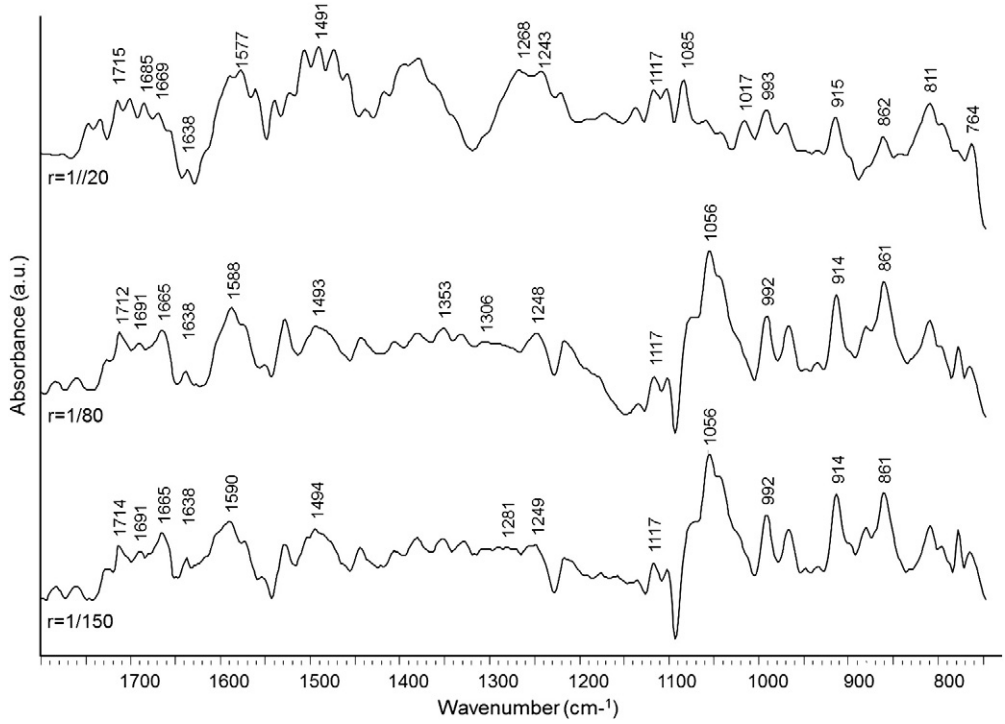

Fig. 9. Difference spectra {(tRNA solution + allicin solution) − tRNA solution} of allicin–DNA complexes in the region of 1800–700 cm^{-1}.

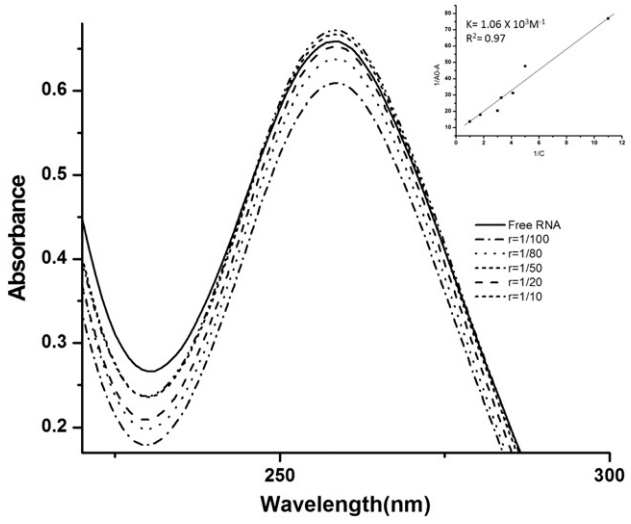

Fig. 10. UV–visible spectra of free tRNA and tRNA–allicin complexes at 260 nm. Plot of $1/(A_0 - A)$ versus $1/C$ for tRNA and its drug complexes, where A_0 is the initial absorption of tRNA and A is the recorded absorption at different drug concentrations.

4. Conclusion

The results demonstrated that allicin treatment inhibited the proliferation of A549, non- small lung cancer cell in a dose-dependent manner. Further study showed that allicin binds DNA via thymine reactive sites located in the minor groove of DNA double helix. In case of allicin binding with tRNA, its major effect was seen on uracil and guanine nitrogenous bases. Some degree of external binding with phosphate backbone has also been observed in both DNA–allicin and tRNA–allicin complex formation. Absorption spectroscopy resulted in hypochromism after allicin complexation to both DNA and RNA. This is suggestive of base binding and helix contraction of nucleic acid structure upon binding with allicin. In view of the anticancer effect of allicin, these results might contribute in deciphering the underlying mechanism of allicin in the exertion of its anti-cancer effect.

Supplementary data to this article can be found online at http://dx.doi.org/10.1016/j.bbagen.2013.09.007.

Conflict of interest

No financial, personal or other conflict of interest exists.

Acknowledgement

The authors thank Director, National Physical Laboratory for granting the permission for publication of the work. G.T. is thankful to Indian Council of Medical Research and S.P. is thankful to Council of Scientific and Industrial Research for providing financial support.

References

[1] G. Hahn, in: H.P. Koch, L.D. Lawson (Eds.), Garlic: the science and therapeutic application of Allium sativum L. and related species, 2nd edn, Williams and Wilkins, Baltimore, 1996, pp. 1–24.
[2] C. Cavallito, J.H. Bailey, Allicin, the antibacterial principal of *Allium sativum*. Isolation, physical properties and antibacterial action, J. Am. Chem. Soc. 66 (11) (1944) 1951–1952.
[3] R.R. Cutler, P. Wilson, Antibacterial activity of a new, stable, aqueous extract of allicin against methicillin-resistant *Staphylococcus aureus*, Br. J. Biomed. Sci. 61 (2) (2004) 71–74.
[4] J.Y. Chan, A.C. Yuen, R.Y. Chan, S.W. Chan, A review of the cardiovascular benefits and antioxidant properties of allicin, Phytother. Res. (2012), http://dx.doi.org/10.1002/ptr.4796.
[5] H. Shirzad, F. Taji, M. Rafieian-Kopaei, Correlation between antioxidant activity of garlic extracts and WEHI-164 fibrosarcoma tumor growth in BALB/c mice, J. Med. Food 14 (9) (2011) 969–974.
[6] T. Mirona, M. Wilcheka, A. Sharpb, Y. Nakagawac, M. Naoic, Y. Nozawac, Y. Akaoc, Allicin inhibits cell growth and induces apoptosis through the mitochondrial pathway in HL60 and U937 cells, J. Nutr. Biochem. 19 (2008) 524–535.
[7] S. Oommen, R.J. Anto, G. Srinivas, D. Karunagaran, Allicin [from garlic] induces caspase-mediated apoptosis in cancer cells, Eur. J. Pharmacol. 485 (2004) 97–103.
[8] S.Y. Park, S.J. Cho, H. Kwon, K.R. Lee, D.K. Rhee, S. Pyo, Caspase-independent cell death by allicin in human epithelial carcinoma cells: involvement of PKA, Cancer Lett. 222 (2005) 123–132.
[9] S.K. Rai, M. Sharma, M. Tiwari, Synthesis, DNA binding, and cytotoxic evaluation of new analogs of diallyldisulfide, an active principle of garlic, Bioorg. Med. Chem. 16 (2008) 7301–7309.
[10] F.H. Fry, N. Okarter, C. Baynton-Smith, M.J. Kershaw, N.J. Talbot, C. Jacob, Use of a substrate/alliinase combination to generate antifungal activity in situ, J. Agric. Food Chem. 53 (2005) 574–580.
[11] N. Hasan, M.U. Siddiqui, Z. Toossi, S. Khan, J. Iqbal, N. Islam, Allicin-induced suppression of *Mycobacterium tuberculosis* 85B mRNA in human monocytes, Biochem. Biophys. Res. Commun. 355 (2007) 471–476.
[12] A. Maréchal, P.R. Rich, Water molecule reorganization in cytochrome c oxidase revealed by FTIR spectroscopy, Proc. Natl. Acad. Sci. 108 (2011) 8634–8638.
[13] F. Garczarek, K. Gerwert, Functional waters in intraprotein proton transfer monitored by FTIR difference spectroscopy, Nature 439 (2006) 109–112.
[14] I.M. Khan, A. Ahmad, M.F. Ullah, Synthesis, spectroscopic investigations, antimicrobial and DNA binding studies of a new charge transfer complex of o-phenylenediamine with 3,5-dinitrosalicylic acid, Spectrochim. Acta A Mol. Biomol. Spectrosc. 102 (2013) 82–87.
[15] D.R. Whelan, K.R. Bambery, P.H. Mark, J.T. Max, D.D. McNaughton, B.R. Wood, Monitoring the reversible B to A-like transition of DNA in eukaryotic cells using Fourier transform infrared spectroscopy, Nucleic Acids Res. 39 (13) (2011) 5439–5448.
[16] I.M. Johnson, H. Prakash, J. Prathiba, R. Raghunathan, R. Malathi, Spectral analysis of naturally occurring methylxanthines [theophylline, theobromine and caffeine] binding with DNA, PLoS One 7 (12) (2012), http://dx.doi.org/10.1371/journal.pone.0050019.
[17] S. Nafisi, R. Namdar, Molecular aspects on the specific interaction of homoisoflavonoids to DNA, J. Photochem. Photobiol. B Biol. 117 (2012) 207–213.
[18] J.F. Neault, H.A. Tajmir-Riahi, RNA–diethylstilbestrol interaction studied by Fourier transform infrared difference spectroscopy, J. Biol. Chem. 272 (1997) 8901–8906.
[19] A.A. Ouameur, P. Bourassa, H.A. Tajmir-Riahi, Probing tRNA interaction with biogenic polyamines, RNA 16 (2010) 1968–1979.
[20] J. Glasel, Validity of nucleic acid purities monitored by 260 nm/ 280 nm absorbance ratios, Biotechniques 18 (1995) 62–63.
[21] R. Vijayalakshmi, M. Kanthimathi, V. Subramanian, U.N. Balachandran, DNA cleavage by a Chromium [III] complex, Biochem. Biophys. Res. Commun. 271 (2000) 731–734.
[22] S. Alex, P. Dupuis, FTIR and Raman investigation of cadmium binding by DNA, Inorg. Chim. Acta 157 (1989) 271–281.
[23] C.D. Kanakis, P.A. Tarantilis, C. Pappas, J. Bariyanga, H.A. Tajmir-Riahi, M.G. Polissiou, An overview of structural features of DNA and RNA complexes with saffron compounds: Models and antioxidant activity, J. Photochem. Photobiol. B Biol. 95 (2009) 204–212.
[24] Optical Absorption Spectroscopy, in: K. Connors (Ed.), Binding Constants: The Measurement of Molecular Complex Stability, John Wiley & Sons, New York, 1987, pp. 141–188.
[25] F. Adnet, J. Liquier, E. Taillandier, M.P. Singh, K.E. Rao, J.W. Lown, FTIR study of specific binding interactions between DNA minor groove binding ligands and polynucleotides, J. Biomol. Struct. Dyn. 10 (1992) 565–575.
[26] J. Liquier, A. Mchami, E. Taillandier, FTIR study of netropsin binding to poly d(A-T) and Poly dA. Poly dT, J. Biomol. Struct. Dyn. 7 (1) (1989) 119–126.
[27] L.S. Glass, B. Nguyen, K.D. Goodwin, C. Dardonville, W.D. Wilson, E.C. Long, M.M. Georgiadis, Crystal structure of a trypanocidal 4,4′-bis(imidazolinylamino)diphenylamine bound to DNA, Biochemistry 48 (25) (2009) 5943–5952.
[28] R.T. Yassaka, H. Inagaki, T. Fujino, K. Nakatani, T. Kubo, Enhanced activation of the transient receptor potential channel TRPA1 by ajoene, an allicin derivative, Neurosci. Res. 66 (2010) 99–105.
[29] Q. Li, P. Yang, H. Wang, M. Guo, Diorganotin [IV] antitumor agent. [C, H,], SnC12 [phen]/nucleotides aqueous and solid-state coordination chemistry and its DNA binding studies, J. Inorg. Biochem. 64 (1996) 181–195.
[30] Y.N. Xiao, C.X. Zhan, Studies on the interaction of DNA and water-soluble polymeric Schiff base–nickel complexes, J. Appl. Polym. Sci. 84 (5) (2002) 887–893.